Biogeosciences Discuss., https://doi.org/10.5194/bg-2017-499
Manuscript under review for journal Biogeosciences
Discussion started: 14 December 2017

Biogeosciences Discussions Open Access EGU

A new procedure for processing eddy-covariance data to better quantify atmosphere-aquatic ecosystem CO_2 exchanges

Tatsuki Tokoro[1,2] Tomohiro Kuwae[1]

[1]Coastal and Estuarine Research Group, Port and Airport Research Institute, 3-1-1 Nagase, Yokosuka 239-0826, Japan

[2]Present address: Marine Macrophyte Ecosystem Group, National Research Institute of Fisheries and Environment of Inland Sea, 2-17-5, Hatsukaichi 739-0452, Japan

Correspondence to: T. Tokoro (tokoro-t@ipc.pari.go.jp)

Abstract. The capture of carbon by aquatic ecosystems and its sequestration in sediments has been studied as a potential method for mitigating the adverse effects of climate change. However, the evaluation of in situ atmospheric CO_2 fluxes is challenging because of the difficulty in making continuous measurements over areas and for periods of time that are environmentally relevant. The eddy covariance (EC) method is the most promising approach to address this concern with the measurement of atmospheric CO_2 fluxes. However, methods to process the data obtained from EC measurements are still being developed, and the estimated air-water CO_2 fluxes have large uncertainties and differ from those obtained using conventional methods. In this study, we improved the post-processing procedure for the EC method to reduce the uncertainty in the measured air-water CO_2 fluxes. Our new procedure efficiently removes erroneous fluxes using a combination of filtering methods based on the received signal strength indicator of the EC sensor, the normalized standard deviation of

Biogeosciences Discuss., https://doi.org/10.5194/bg-2017-499
Manuscript under review for journal Biogeosciences
Discussion started: 14 December 2017

atmospheric CO_2 and water vapor concentrations, and a high-pass filter. Our procedure is easier to apply to EC measurements than existing correction methods. The improved EC fluxes did not always agree with those obtained by using conventional methods (e.g., the bulk formula method), but this difference was attributable to the difference of measurement heights and the effect on the measured fluxes of the physical and biological properties of the water surface (e.g., the presence of vegetation on the water surface and the temperature gradient in the overlying atmospheric layer). Because the measurement height and the spatiotemporal scales of the flux measurement depend on the applied method, it is essential to select the appropriate method for studies related to CO_2 fluxes and to the determination of ecosystem-atmospheric CO_2 interactions and the role of aquatic ecosystems in mitigating the adverse effects of climate change.

1 Introduction

Aquatic environments are considered critical to the mitigation of adverse climate change effects because of their ability to store atmospheric CO_2. Previous studies have estimated that the ocean absorbs approximately one-fourth of the CO_2 emitted by anthropogenic activities (IPCC, 2013). However, the effect of shallow aquatic ecosystems on atmospheric CO_2 remains a controversial topic. Several previous studies have concluded that shallow aquatic ecosystems are sources of atmospheric CO_2 after taking account of carbon inputs from land (e.g. Gazeau et al., 2005; Borges et al., 2006; Chen et al., 2013). In contrast, some autotrophic, shallow aquatic ecosystems have been reported to be net sinks for atmospheric CO_2 (e.g. Schindler et al., 1997; Tokoro et al., 2014).

In situ measurements of atmospheric CO_2 fluxes are necessary for precise analysis

Biogeosciences Discuss., https://doi.org/10.5194/bg-2017-499
Manuscript under review for journal Biogeosciences
Discussion started: 14 December 2017

of carbon cycling in aquatic environments. CO_2 fluxes in aquatic environments are difficult to determine because of the variability of several factors, including concentrations of CO_2 in the water and air and the physical characteristics of the atmosphere and water surface. Several methods have been proposed for measuring in situ CO_2 fluxes. Because each of these methods works best at a different combination of spatial and temporal scales and is associated with different costs and technical difficulties, a variety of methods have been applied to different aquatic environments (e.g. oceans, estuaries, and lakes) to assess rates of aquatic carbon cycling.

Methods of estimating air-water CO_2 fluxes can be assigned to one of two categories: (1) indirect estimations based on CO_2 concentration gradients just below the water surface (Lewis and Whitman, 1924) or from the renewal rate of a very small body of water (Danckwerts, 1951), and (2) direct estimations. With either of the indirect methods, the CO_2 flux is calculated from the product of the difference in the CO_2 fugacity (fCO_2) between air and water, the CO_2 solubility, and a physically regulated parameter called the transfer velocity. Because the transfer velocity cannot be estimated directly, empirical and hydrodynamic models for estimating transfer velocity have been proposed (Garbe et al., 2013).

At the present time, the empirical model is primarily used for evaluating aquatic CO_2 fluxes because of the difficulty in applying the hydrodynamic model. In the empirical model, the regulating factor for transfer velocity has been identified from several direct CO_2 measurements by using tracers such as ^{14}C and SF_6 (e.g. Broecker and Peng 1982; Ho et al., 2014) or water-tank experiments (e.g. Komori et al., 1993). Based on these results, several empirical equations have been formulated. The wind speed above the water surface is a metric of one regulating factor (e.g. Liss and

71 Merlivat, 1986; Wanninkhof, 1992; Ho et al., 2006). In the case of shallow systems,
72 water velocity fields and depths have been used to estimate the gas transfer velocity
73 (O'Conner and Dobbins, 1958; Borges et al., 2004). In this study, the method using such
74 empirical model for estimating aquatic CO_2 flux is defined as the Bulk Formula method
75 (BF method).

76 However, application of the BF method is limited because of its poor temporal and
77 spatial coverage. Moreover, in previous studies, air-water CO_2 fluxes have been
78 determined mostly as snapshots that did not account for diurnal changes or annual
79 cycles, the result being considerable uncertainty and bias (Kuwae et al., 2016). In
80 brackish environments in particular, temporal variability of water fCO_2 is significant,
81 whereas the carbonate buffer effect is weak, and the fluctuations of fCO_2 become very
82 large (Zeebe and Wolf-Gladrow, 2001). Use of BF methods to carry out a
83 comprehensive analysis of dynamic carbon cycling in aquatic environments with large
84 spatial and temporal variability would therefore be very costly and require much effort.

85 Another method for evaluating the air-water CO_2 fluxes is direct measurement of in
86 situ fluxes, which involves use of a chamber floating on the water surface (e.g.
87 Frankignoulle, 1988; Tokoro et al., 2008) and eddy covariance devices (vide infra). The
88 floating chamber method is used to determine the air-water CO_2 flux from continuous
89 measurements of CO_2 concentrations in the air inside a hollow, box-shaped device
90 floating on the water surface. Although this method is the easiest of the direct methods
91 to use in shallow coastal waters because of its relative simplicity, like the BF method, it
92 is poorly suited for obtaining long-term measurements over wide areas.

93 The eddy covariance (EC) method, which is commonly used to determine mass and
94 heat fluxes in terrestrial environments, has recently been used to estimate air-water

fluxes of greenhouse gases (e.g. Lee et al., 2004). The determination of the EC CO_2 flux is based on the micro-meteorological behavior of atmospheric eddy diffusion and is calculated from the covariance of atmospheric CO_2 concentrations and vertical wind speeds measured at high frequency (more than 10 Hz). Because EC measurements can be performed automatically and represent the flux over a large area, the EC method can be used to obtain a detailed analysis of CO_2 fluxes.

Despite the promise of EC measurements, application of the EC method in aquatic environments remains challenging (Tsukamoto et al., 2004; Rutgersson and Smedman, 2010; Vesala, 2012; Blomquist et al., 2013; Kondo et al., 2014; Ikawa and Oechel, 2014; Landwehr et al., 2014). The difficulty of making aquatic EC measurements is that the air-water CO_2 flux is small compared with the air-land CO_2 flux (Vesala, 2012; Landwhehr et al., 2014). The main technical problem with the EC method is cross sensitivity, which reflects the interference between the atmospheric CO_2 and H_2O measurements caused by spectrometric error (Kohsiek et al., 2000; Prytherch et al., 2010; Kondo et al., 2014; Landwehr et al., 2014). A procedure based on the relationship between atmospheric CO_2 concentration and relative humidity called the PKT correction has been proposed to correct for the effects of cross sensitivity (Prytherch et al., 2010). However, the PKT correction is not always effective. Past studies have revealed that cross sensitivity is reduced only after application of certain operational procedures such as cleaning the optical lens of the sensor (Ikawa and Oechel, 2014; Kondo et al., 2014) and drying the sample gas (Landwhehr et al., 2014).

There are several problems in addition to cross sensitivity in using EC measurements in aquatic environments. The uncertainty of EC measurements has been attributed to the spatial and temporal heterogeneity of water (Mørk et al., 2014). The EC

flux is calculated as the average within a measurement area called the "footprint", which can range from several hundred meters to several kilometers windward from the measurement point (Schuepp et al., 1990). Therefore, EC fluxes at heterogeneous water sites are different from the fluxes determined by methods that estimate the CO_2 flux in an area of only several square meters (e.g., the BF method and floating chamber method). The EC flux is an average flux over a certain time interval (approximately several tens of minutes) (Lee et al., 2004), whereas the BF method estimates the flux at the time of sampling. Thus, EC fluxes estimated at sites where fluxes are temporally variable also differ from fluxes obtained using other methods. Furthermore, the inflow of terrestrial air into the measurement site can generate uncertainty in the flux measurement because the atmospheric CO_2 concentration over terrestrial vegetation may differ significantly from the concentration over water. The inflow of terrestrial air can cause unnatural temporal changes in the atmospheric CO_2 concentration and spatial heterogeneity at the measurement site. It is therefore necessary to account for the characteristics of the aquatic environment and apply appropriate post-processing (PP) procedures (Leinweber et al., 2009) to avoid large uncertainties or biases in EC flux calculations.

In this study, we developed a PP procedure for EC aquatic measurements. This PP procedure involves the exclusion of erroneous data and correction of unnatural changes in the atmospheric CO_2 using a series of data-filtering steps. The new process is based on the idea that cross sensitivity and environmental heterogeneity during flux measurement cause spikes, drifts, offsets, and long-term variation in the CO_2 and H_2O raw data. We compared the results calculated with our new PP procedure to those obtained using conventional EC PP procedures along with BF flux data as an example

of a frequently used method. We then discuss the differences between the conventional BF and EC fluxes with respect to atmospheric and environmental characteristics.

2 Methods

2.1 Field measurements

Continuous EC measurement data were used for the evaluation of the PP procedure and the analysis of atmospheric-aquatic ecosystem CO_2 exchange. The data were collected from a brackish lagoon in Japan (the Furen Lagoon, Fig. 1) from 28 May to 21 October 2014, during which time the water surface was not frozen. Most of the study area (57.4 km^2) is covered by seagrass meadows (mainly *Zostera marina*). The water is shallow (1–2 m), except in a channel that connects the eastern and western basins of the lagoon (depth = approximately 5 m). Freshwater flows into the western basin through several rivers that run through the surrounding grass farms, and seawater is exchanged through the lagoon mouth, which opens to the Okhotsk Sea. A previous study has found that the air-water CO_2 flux in the lagoon is affected by changes of salinity caused by the inflow of river water and tides as well as by changes of dissolved inorganic carbon resulting from biological processes such as photosynthesis (Tokoro et al., 2014). The measurement platform was built at the same site used in the study of Tokoro et al. (2014) (N43° 19.775', E145° 15.463'); the effects of photosynthesis and changes in salinity are most notable at this location in the lagoon (Tokoro et al., 2014).

The EC devices used in this study were as follows. Atmospheric CO_2 concentrations and water vapor were measured with an open-path sensor (LI-7500A, LI-COR, USA). The three-dimensional (3D) wind velocity, air temperature, and atmospheric pressure were measured with a 3D acoustic Doppler velocimeter (CSAT-3, Campbell Scientific,

Biogeosciences Discuss., https://doi.org/10.5194/bg-2017-499
Manuscript under review for journal Biogeosciences
Discussion started: 14 December 2017

166 USA). The data were logged and managed by a SMARTFlux system (LI-COR). The
167 open-path sensor and the wind velocimeter were attached to the platform approximately
168 3.0–5.5 m above the water surface (the height varied with the tide). The sampling rate
169 for all data was 10 Hz, and the fluxes (CO_2, water vapor, and heat) were calculated as
170 averages over 30-min intervals. Batteries and solar panels were attached to the platform
171 as a power source. Battery replacement, data collection, and device maintenance were
172 performed approximately every two weeks. Water temperature and salinity were
173 measured continuously with a conductivity-temperature sensor (Compact-CT, Alec,
174 Japan).

175 **2.2 Calculation of fluxes using the conventional PP procedure (PP1)**

176 The air-water CO_2 flux (F) was calculated every 30-min using the following equation:
177

178 $$F = \overline{\rho_c' w'} \cdot F_1 + \mu \frac{\rho_c}{\rho_d} \overline{\rho_v' w'} \cdot F_1 + \rho_c \left(1 + \mu \frac{\rho_v}{\rho_d}\right) \frac{\overline{T_a' w'}}{T_a} \cdot F_2 , \quad (1)$$

179

180 where the coefficients F_1 and F_2 are correction terms based on the transfer functions that
181 correct for the frequency attenuation of the air-sea CO_2 flux caused by the response time
182 of the sensor, path-length averaging, sensor separation, signal processing, and flux-
183 averaging time (Massman, 2000). The first term on the right-hand side of Eq. (1) is the
184 product of F_1 and the uncorrected air-sea CO_2 flux calculated as the covariance of the
185 CO_2 density ρ_c and the vertical wind speed w (the bar and the prime indicate the mean
186 and the deviation from the mean, respectively). The second and third terms are the
187 Webb-Pearman-Leuning correction of latent heat and sensible heat, respectively (Webb

Biogeosciences Discuss., https://doi.org/10.5194/bg-2017-499
Manuscript under review for journal Biogeosciences
Discussion started: 14 December 2017

et al., 1980). The other variables in Eq. (1) are defined as follows: ρ_d = dry air density; ρ_v = water vapor density; T_a = air temperature; and μ = ratio of the molar weight of dry air to that of water vapor. The wind speed was corrected by using a double rotation to make the average vertical wind speed zero during the 30-min time interval (Lee et al., 2004). The footprint (measurement area) depends on several factors, including the measurement height, wind speed, atmospheric stability, and measurement site roughness (10^{-4} cm) (Schuepp et al., 1990). This footprint ranged from several hundred square meters to several square kilometers on the windward side of the measurement site.

The deviation of each parameter in Eq. (1) from the 30-min average was calculated by subtracting the 30-min average from the instantaneous data after deleting obviously erroneous data (e.g., negative values of CO_2 or water vapor concentration). Other corrections to the raw data included coordinate rotation of the 3D wind component (double rotation; Lee et al., 2004), time lag of the measurement due to the separation of the CO_2 sensor and the wind velocimeter (covariance maximization; Lee et al., 2000), exclusion of wind data contaminated by the wind velocimeter flame, and correction of the measurement noise (statistical tests of Vickers and Mahrt, 1997) based on the default settings of the data management software (EddyPro 5.1.1, LI-COR).

2.3 Calculation of flux using our new PP procedure (PP2)

After calculating the EC flux using the conventional PP procedure (PP1) described in Sect. 2.2, we recalculated the EC flux using our new procedure (PP2; Fig. 2). The PP2 procedure is mainly based on filtering and excluding erroneous data rather than on the PKT method of data correction. The PP2 procedure is also focused on aquatic environments in which the spatial and temporal variations in atmospheric CO_2 are large.

The PP2 procedure combines a series of filtering methods based on the received signal strength indicator (RSSI) of the EC sensor, the normalized standard deviations (nSDs) of the atmospheric CO_2 and water vapor concentrations, and high-pass (HP) filtering.

The RSSI is one of the data concurrently obtained from the CO_2 sensor of the EC measurement instrumentation and indicates the available signal strength of the sensor. This parameter has been used for evaluating measurement validation of objective gases such as methane. In this study, we used the RSSI to filter the CO_2 data because both CO_2 and methane absorb infrared radiation. First, data in the 30-min time series were excluded if their RSSI was low. The RSSI threshold for exclusion was set to 90 %, because this percentage was sufficiently high to identify valid CO_2 concentrations and allowed most of the measurement data (~81 %) to be retained. This 90 % threshold was also recommended as the quality criterion for the LI-7700 methane analyzer (LI-COR), which has been used to measure methane concentrations. (http://www.licor.com/env/newsline/2012/04/overcoming-the-challenges-of-open-path-methane-measurements-with-the-li-7700/).

Second, the criteria for excluding erroneous fluxes were identified. Erroneous fluxes were identified based on unnatural spikes, jumps, and shifts in the data. Outliers were excluded based on three statistical parameters: (1) the normalized standard deviation, nSD (i.e. the SD over a 30-min period divided by the average value for the entire measurement period after RSSI filtering; (2) skewness; and (3) the absolute value of kurtosis. Each of these threshold values was determined after the top four outliers for each parameter were excluded; the raw data (CO_2 concentration, wind speed) associated with the top four outliers were assumed to be erroneous changes that would not happen naturally.

Biogeosciences Discuss., https://doi.org/10.5194/bg-2017-499
Manuscript under review for journal Biogeosciences
Discussion started: 14 December 2017

235 Finally, HP filtering was applied to the calculation of the deviations from the mean
236 of each parameters in Eq. (1). This procedure corrected relatively long-term (several
237 minutes to 30 minutes) variations in CO_2 or water vapor concentrations that were
238 independent of eddy fluctuations and were caused by the temporal and spatial
239 heterogeneity of the atmospheric mass. HP filtering is often applied to measurements in
240 a complex environment; however, incorrect application of HP filtering results in
241 underestimation of fluxes (Lee et al., 2004). HP filtering was applied by using an
242 exponential moving average as follows:
243

244
$$\begin{aligned} x_i' &= A\left(x_i - x_{i-1}\right) + A x_{i-1}' \\ A &= \exp\left(-1/\tau \cdot f\right) \end{aligned}, \qquad (2)$$

245

246 where x_i and x_i' are an instantaneous datum and deviation from the mean at time i,
247 respectively. The parameter τ is the time constant of the exponential moving average,
248 which was determined to be 150 s in a previous study (McMillan, 1988), and f is the
249 sampling frequency (10 Hz). HP filtering was applied to all of the measured data (i.e.,
250 3D wind velocity, air temperature, CO_2 and water vapor concentrations, and
251 atmospheric pressure).

252 **2.4 Measurement of fluxes using the BF method**

253 BF flux measurements were performed during the daytime on 29 May, 15 July, and 21
254 September 2014 for comparison with the EC measurements. In the BF method, flux is
255 calculated as follows:
256

Biogeosciences Discuss., https://doi.org/10.5194/bg-2017-499
Manuscript under review for journal Biogeosciences
Discussion started: 14 December 2017

$$F = kS\left(fCO_{2water} - fCO_{2air}\right), \quad (3)$$

where k is the transfer velocity, which was calculated using one or another of the following three empirical equations. The first was the equation of Wanninkhof (1992) (W92). Because this equation was constructed using tracer methodology under oceanic conditions, it might be inappropriate to our measurements because of the differences in fetch and water depth. However, this equation is very commonly used in a variety of oceanographic CO_2 flux studies, including coastal measurements. We therefore used it for comparison. The second equation was that of Borges et al. (2004) (B04), which has been applied in an estuarine study that involved use of the floating chamber method. This equation makes use of the current velocity in addition to the wind speed. The third equation was that of Mørk et al., (2014) (M14), which was formulated to characterize the transfer velocity in a fjord for use with the EC method. Thus, the second and third equations can be used to characterize coastal gas transfer velocity. The wind speed for the gas transfer velocity was measured by the EC device and normalized to a height of 10 m from the water surface using a logarithm law (Kondo, 2000). The current speed and depth were measured by the sensors attached to the platform (Compact-TC and Compact-EM, Alec, Japan). The final CO_2 flux was calculated as the weighted average of the fluxes measured within the EC footprint (Schuepp et al., 1990).

The parameter S is the dissolution coefficient of CO_2, which was estimated from the water temperature and salinity (Weiss, 1974). The parameters fCO_{2water} and fCO_{2air} are the fugacity of water and atmospheric CO_2, respectively. Water temperature and salinity were measured with a handheld conductivity-temperature-depth sensor (ACTD-DF, JFE Advantech, Japan). The water samples used to determine fCO_{2water} were collected just

below the water surface (up to 20 cm below the water surface) to measure the concentration of CO_2 where direct gas exchange with air occurs. The sampling was performed within the EC footprint to minimize the effect of spatial heterogeneity when comparing the BF and EC fluxes. The sampling points were determined from the wind direction and the distance from the platform measured using a hand-held GPS unit (Venture HC, Garmin, USA; see Table S1). The water fCO_2 was determined from the total alkalinity and the dissolved inorganic carbon content of the water sample using a batch-type carbonate measurement system (ATT-05, Kimoto electrics, Japan) and the CO2SYS program (Pierrot et al., 2006).

3 Results

3.1 PP1 data

During the measurement period, 4464 flux data points corresponding to 2232 hours were obtained; 1971 of those data points (44 %) were excluded as erroneous data after PP1 application. The mean and SD of the EC CO_2 fluxes were −1.93 and 52.4 μmol m^{-2} s^{-1}, respectively. Figure 3(a) shows the retained CO_2 flux data.

The largest positive CO_2 flux (release to atmosphere) was 156.51 μmol m^{-2} s^{-1} at 2:00 on 23 June (day 56). The largest negative CO_2 flux (uptake of atmospheric CO_2) was −217.93 μmol m^{-2} s^{-1} at 22:00 on 4 October (day 129). These fluxes were more than three orders of magnitude larger than the magnitude of the average of the measured EC fluxes. Figure 4 shows the instantaneous atmospheric CO_2 concentration, water vapor concentration, and the cumulative covariance between CO_2 and vertical wind speed during the times when the CO_2 fluxes were most positive or most negative.

Biogeosciences Discuss., https://doi.org/10.5194/bg-2017-499
Manuscript under review for journal Biogeosciences
Discussion started: 14 December 2017

304 Spikes and discontinuities were observed in the atmospheric CO_2 and water vapor
305 concentrations, despite the prior de-spiking process applied by the data management
306 system. The cumulative covariance indicated that the covariance at certain periods (0–5
307 min) contributed significantly to the total cumulative covariance.

308 **3.2 PP2 data**

309 The EC CO_2 flux data subjected to PP2 (RSSI, nSD, and HP filtering) are shown in Fig.
310 3(b). Of the 2493 total data points remaining after PP1, approximately 234 (9 %) were
311 excluded by RSSI filtering. Subsequent nSD filtering removed 426 additional data
312 points (17 %); approximately 73 % of the measurement data remained after this
313 filtering. The mean and SD of EC CO_2 flux after PP2 were −0.54 and 2.2 μmol m^{-2} s^{-1},
314 respectively.

315 The nSD threshold was calculate using the averages of the CO_2 and water vapor
316 concentrations for the entire measurement period after RSSI filtering (CO_2: 16.02 mmol
317 m^{-3}, vapor: 548.10 mmol m^{-3}). The nSD threshold value obtained from the average
318 values was 0.050. Other thresholds were 0.48 for skewness and 3.1 for the absolute
319 value of kurtosis. Among these comparisons, the nSD was determined to provide the
320 best threshold for the measurement data because the number of data remaining after
321 filtering was the largest for the nSD (nSD: 1661 [74 %], skewness: 422 [19 %], and the
322 absolute value of kurtosis: 445 [20 %]). The nSD filtering resulted in the exclusion of
323 137 (6 %) of the CO_2 data points and 569 (25 %) of the water vapor data points. Figure
324 5 shows the three parameters for the EC CO_2 flux data.

325 HP filtering decreased the absolute values of some CO_2 fluxes (Fig. 6). Most of the
326 data were not changed very much by HP filtering; however, HP filtering decreased the

absolute values of some fluxes. Figure 7 shows an example of the results of filtering atmospheric CO_2 concentrations as well as the cumulative covariance of the atmospheric CO_2 concentrations and vertical wind speed (measured at 8:00 on August 21 [day 84]). These data were not excluded by the RSSI and nSD filtering (RSSI = 100 %, nSD of CO_2 = 9.84×10^{-3}, nSD of H_2O = 2.07×10^{-2}). The concentration of atmospheric CO_2 showed a trend over the 30-min time interval, the indication being that the block average could not extract appropriate eddy movements from the time-series data. The cumulative covariance of the block averaging (BA) was unusually large; after HP filtering, the values were more reasonable because filtering successfully excluded deviations caused by the variation for about 10-min of atmospheric CO_2 concentrations.

3.3 BF data

The measured BF fluxes showed spatial and seasonal variations (see Table S1). The means and SDs obtained by using the three gas transfer velocity equations to analyze the weighted averages of the BF CO_2 flux data were 0.44 ± 0.33 μmol m^{-2} s^{-1} (n = 15) on 29 May (day 1), 2.10 ± 1.58 μmol m^{-2} s^{-1} (n = 14) on 15 July (day 48), and −0.11 ± 0.13 μmol m^{-2} s^{-1} (n = 9) on 21 September (day 115). The differences in the number of data reflect problems during the measurements, such as inadequate water depth and problems with the water-depth sensor. Except for the measurements on 15 July, the difference between the results obtained with the three gas transfer velocity equations were not significant.

4 Discussion

Our new filtering method, PP2, successfully excluded erroneous outliers. The SD was

decreased by a factor of 24 (52.4 μmol m^{-2} s^{-1} in PP1 to 2.2 μmol m^{-2} s^{-1} in PP2). The atmospheric CO_2 uptake rate calculated via PP1 measurements (–1.93 μmol m^{-2} s^{-1}) was reduced in magnitude by 72 % after PP2 to –0.54 μmol m^{-2} s^{-1}. This uptake rate is more consistent with the range of atmospheric CO_2 uptake rates reported in previous studies (e.g. Borges et al., 2005; Chen et al., 2013; Laruelle et al., 2013). The most negative CO_2 flux ever reported was –1.08 μmol m^{-2} s^{-1} during spring in the Baltic Sea (Chen et al., 2013).

The exclusion of erroneous outliers by PP2 also contributed to the time-series analysis. The power spectra of the EC CO_2 fluxes after PP1 evidenced large, noise-like fluctuations at high frequencies (Fig. 8), and thus any suggestion of peaks in the time series was obscured. After PP2, however, the noise-like fluctuations were smaller, and two peaks associated with semi-diurnal (~12.5 h) and diurnal (~24 h) time intervals were apparent. The fCO_2 variations in the lagoon, which are among the parameters that regulate air-water CO_2 fluxes, have been confirmed to be related to mixing of lagoon water with freshwater coming from rivers and with biological processes such as photosynthesis (Tokoro et al., 2014). Given that the former and latter phenomenon are caused by the semi-diurnal tidal cycle and diel changes of irradiance, respectively, the peaks in the power spectra are consistent with the results of Tokoro et al. (2014). This consistency is a good demonstration of the utility of the PP2.

The EC data that were much different from the BF results were excluded by the PP2 (Fig. 9). The remaining EC fluxes in May and September seemed to agree well with the BF fluxes. We believe that one of the reasons that the results were comparable was the improvement in the accuracy of the EC fluxes with the use of PP2. Another reason was our strategy of making BF measurements at multiple points within the EC footprint to

filter out the noise associated with the spatial heterogeneity of the BF fluxes. In July, the BF fluxes estimated with the W92 seemed to be the most consistent with the EC fluxes. This similarity indicates that the effect of currents in the B04 and the effect of early-breaking waves in the M14 were overestimated at our measurement site.

However, the EC fluxes estimated with PP2 did not always agree with the BF fluxes. Because the fCO_{2water} is theoretically never negative, a theoretical maximum negative BF flux can be calculated by arbitrarily setting fCO_2 equal to zero. The maximum negative flux calculated in this way (with M14) was −6.16 μmol m^{-2} s^{-1} at 15:00 on 30 May (day 2), when the maximum wind speed was recorded (11.9 m/s). Forty-seven EC flux data points (3 % of all data) indicated even lower fluxes. Moreover, the mean of the EC fluxes with PP2 (–0.54 μmol m^{-2} s^{-1}) was more negative or almost the same as the mean of the theoretical BF fluxes (–0.26 μmol m^{-2} s^{-1} in, –0.55 μmol m^{-2} s^{-1}, and –0.43 μmol m^{-2} s^{-1} estimated with W92, B04, and M14, respectively). Because actual BF fluxes include less negative as well as positive fluxes, these EC fluxes cannot be explained by only the BF fluxes.

Similar inconsistencies between air-water CO_2 fluxes calculated with the EC method and other conventional methods have been reported in several studies (e.g., Tsukamoto et al., 2004; Rutgersson et al., 2010). In the case of coastal measurements, water-side convection due to the vertical temperature difference inside water has been postulated to enhance the gas transfer velocity (Rutgersson et al., 2010). However, such an enhancement was not previously observed with direct flux measurement using a floating chamber at our site (Tokoro et al., 2014). Because of the very shallow water depth (less than 2 m) at our site, we suspect that water-side convection was weak and was not the main reason for the inconsistency of the fluxes.

Assuming that the EC fluxes obtained with PP2 are valid, the discrepancy between the EC and BF fluxes was also postulated to reflect the limitations of the BF method and/or the difference of the measurement height of the BF and EC methods; the former and the latter are at the water surface and the height of the EC devices, respectively. As for the BF method limitaitons, seagrass leaves, which reached the water surface during low tide at the study site, might have affected the physical and chemical conditions at the water surface (Watanabe and Kuwae, 2015). In BF theory, the CO_2 flux is caused by the CO_2 concentration gradient just below the water surface. The BF method should therefore not be applied when seagrass is present on the water surface. A previous study that investigated the radiocarbon isotopic signatures of seagrass at the study site indicated that of the total CO_2 assimilated by the seagrass, 0–40 % (mean = 17 %) originated from the atmosphere and the rest from the water (Watanabe and Kuwae, 2015). The implication is that there is direct uptake of atmospheric CO_2 (rather than uptake through the water column) by seagrass when seagrass leaves are on the water surface. Atmospheric CO_2 is therefore directly taken up within a thin film of water over the seagrass leaves, but this seagrass-driven CO_2 flux is not included in the BF flux calculations.

The fact that the CO_2 flux was larger than the BF flux may have been partly caused by the temperature and CO_2 gradients in the atmospheric layer between the EC measurement height and the water surface. Vertical gradients in air temperature frequently occur because of the large difference in temperature between the atmosphere and water. Indeed, the difference between the temperature at the EC measurement height and the water temperature (ΔT) ranged from +8 °C to −10 °C during the measurement period (Fig. 10). The atmospheric CO_2 concentration was inversely

Biogeosciences Discuss., https://doi.org/10.5194/bg-2017-499
Manuscript under review for journal Biogeosciences
Discussion started: 14 December 2017

421 proportional to air temperature, mainly because of the ideal gas law. The inflow of air
422 masses with different temperatures and CO_2 concentrations from other regions
423 surrounding the lagoon (e.g., terrestrial environments and open sea) could also have
424 contributed to this inverse relationship. We therefore believe that the ΔT caused a
425 vertical gradient in atmospheric CO_2 concentration, the result being a vertical CO_2 flux
426 in accord with Fick's law. Indeed, the absolute values of the EC CO_2 fluxes were large
427 when ΔT was large (Fig. 11b). For example, a large negative EC flux that was more than
428 10 times the maximum negative BF flux was observed when the ΔT was negative and
429 large in magnitude. This phenomenon frequently occurs when a cold air mass overlies a
430 warm air mass (Fig. 11a). The opposite phenomenon is observed when a warm air mass
431 overlies a cold air mass (Fig. 11b). The positive temperature gradient did not result in a
432 large EC flux similar to the flux associated with the negative temperature gradient
433 because the positive temperature gradient produced stable stratification and thereby
434 prevented vertical eddy movement and CO_2 flux, a phenomenon observed in the case of
435 terrestrial EC fluxes at night (Aubinet and Feigenwinter, 2010). Nevertheless, a
436 temperature gradient-driven vertical CO_2 flux may explain the discrepancy between the
437 EC and BF fluxes.

438 In summary, we attribute the discrepancy between the EC and BF fluxes to the
439 following four factors: (1) major technical uncertainties in both methods; (2) differences
440 in measurement location and in the temporal scales of the measurements; (3) limitations
441 of the BF method related to the presence of vegetation on the water surface; and (4) the
442 gradient of atmospheric conditions between the height of the EC measurements and just
443 above the water surface (Table 1). The latter two factors may cause the EC CO_2 flux to
444 be larger than the BF flux in aquatic systems that have large amounts of vegetation or

are located where temperature gradients form in the atmospheric boundary layer. Determination of the contribution of aquatic ecosystems to mitigating the adverse effects of climate change will require consideration of all processes related to atmosphere-aquatic ecosystem exchange. For this purpose, the EC CO_2 flux should be a more robust indicator than the BF flux, which includes only processes related to air-water exchanges. Improving the EC method is therefore essential for a re-evaluation of atmosphere-aquatic ecosystem CO_2 gas exchanges and comprehensive analyses of the contributions of aquatic environments to mitigating the adverse effects of climate change.

Competing interests. The authors declare that they have no conflict of interests.

Acknowledgements. We thank K. Watanabe, H. Moki, E. Miyoshi, and S. Montani for help with the field work and F. Kondo and H. Ikawa for helpful comments. This study was supported by a Grant-in-Aid for Challenging Exploratory Researches (no. 24656316 and 26630251) from the Japan Society for the Promotion of Science and a Strategic R&D Area Project (S-14) of the Environmental Research and Technology Development Fund (Strategic Research on Global Mitigation and Local Adaptation to Climate Change).

References

Aubinet, M. and Feigenwinter, C.: Direct CO_2 advection measurements and the night flux problem, Agr. Forest Meteorol., 150, 651–654, 2010.

Blomquist, B. W., Huebert, B. J., Fairall, C. W., Bariteau, L., Edson, J. B., Hare, J. E.

and McGillis, W. R.: Advances in Air-Sea CO_2 Flux Measurement by Eddy Correlation, Bound-Lay. Meteorol., 152, 245–276, 2013.

Borges, A. V., Vanderborght, J. P., Schiettecatte, L. S., Gazeau, F., Ferrón-Smith, S., Delille, B. and Frankignoulle, M.: Variability of the gas transfer velocity of CO_2 in a macrotidal estuary (the Scheldt), Estuaries, 27, 593–603, 2004.

Borges, A. V., Delille, B., and Frankignoulle, M.: Budgeting sinks and sources of CO_2 in the coastal ocean: Diversity of ecosystems counts, Geophys. Res. Lett., 32, L14601, 2005.

Borges, A. V., Schiettecatte, L. S., Abril, G., Delille, B. and Gazeau, F.: Carbon dioxide in European coastal waters, Estuar. Coast. Shelf S., 70, 375–387, 2006.

Broecker, W. S., and Peng, T-H.: Tracers in the sea, the Lamont-Doherty Geological Observatory, New York, 1982.

Chen, C. T. A., Huang, T. H., Chen, Y. C., Bai, Y., He, X. and Kang, Y.: Air-sea exchanges of coin the world's coastal seas, Biogeosciences, 10, 6509–6544, 2013.

Danckwerts, P. V.: Significant of liquid-film coefficient in gas absorption, Ind. Eng. Chem., 43, 1460-1467, 1951.

Frankignoulle, M.: Field-measurements of air sea CO_2 exchange, Limnol. Ocean., 33, 313-322, 1988.

Garbe, C. S., Rutgersson, A., Boutin, J., de Leeuw, G., Delille, B., Fairall, W., Gruber, N., Hare, J., Ho, D. T., Johnson, M. T., Nightingale, P. D., Pettersson, H., Piskozub, J., Salée, E., and Tsai, W-t.: Transfer across the air-sea interface, in: Open-atmosphere interaction of gases and particles, Springer, Heidelberg, 55-122, 2014.

492 Gazeau, F., Duarte, C. M., Gattuso, J. P., Barrón, C., Navarro, N., Ruiz, S., Prairie, Y. T.,
493 Calleja, M., Delille, B., Frankignoulle, M., and Borges, A. V.: Whole-system
494 metabolism and CO_2 fluxes in a Mediterranean Bay dominated by seagrass beds
495 (Palma Bay, NW Mediterranean), Biogeosciences, 2, 43–60, 2005.
496 Ho, D. T., Law, C. S., Smith, M. J., Schlosser, P., Harvey, M., and Hill, P.: Measurement
497 of air-sea gas exchange at high wind speeds in the Southern Ocean: Implications
498 for global parametrization, Geophys. Res. Lett., 33, L16611, 2006.
499 Ho, D. T., Ferrón, S., Engel, V. C., Larsen, L. G., and Barr, J. D.: Air-water gas
500 exchange and CO_2 flux in a mangrove-dominated estuary, Geophys. Res. Lett.,
501 41, 108-113, 2014.
502 Ikawa, H. and Oechel, C.: Temporal variations in air-sea CO_2 exchange near large kelp
503 beds near San Diego, California, J. Geophys. Res- Oceans, 120, 50–63, 2014.
504 IPCC: Climate Change 2013: The Physical Science Basis. Contribution of Working
505 Group I to the Fifth Assessment Report of the Intergovernmental Panel on
506 Climate Change [Stocker, T. F., D. Qin, G.-K. Plattner, M. Tignor, S. K. Allen, J.
507 Boschung, A. Nauels, Y. Xia, V. Bex and P. M. Midgley (eds.)]. Cambridge
508 University Press, Cambridge, United Kingdom and New York, NY, USA, 2013.
509 Kohsiek, W.: Water vapor cross-sensitivity of open path H_2O/CO_2 sensors, J. Atmos.
510 Ocean. Tech., 17, 299–311, 2000.
511 Komori, S., Nagaosa, R., and Murakami, Y.: Turbulent structure and heat and mass
512 transfer mechanism at a gas-liquid interface in a wind-wave tunnel, Appl. Sci.
513 Res., 51, 423-427, 1993.
514 Kondo, F., Ono, K., Mano, M., Miyata, A. and Tsukamoto, O.: Experimental evaluation
515 of water vapor cross-sensitivity for accurate eddy covariance measurement of

CO_2 flux using open-path CO_2/H_2O gas analysers, Tellus B, 66, 2014.

Kondo, J.: Atmospheric Science near the Ground Surface, University of Tokyo Press, Japan, 2000.

Kuwae, T., Kanda, J., Kubo, A., Nakajima, F., Ogawa, H., Sohma, A. and Suzumura, M.: Blue carbon in human-dominated estuarine and shallow coastal systems, Ambio, 45, 290–301, 2016.

Laruelle, G. G., Dürr, H. H., Lauerwald, R., Hartmann, J., Slomp, C. P., Goossens, N., and Regnier, P. A. G.: Global multi-scale segmentation of continental and coastal waters from the watersheds to the continental margins, Hydrol. Earth. Syst. Sci., 17, 2029-2051, 2013.

Landwehr, S., Miller, S. D., Smith, M. J., Saltzman, E. S. and Ward, B.: Analysis of the PKT correction for direct CO_2 flux measurements over the ocean, Atmos. Chem. Phys., 14, 3361–3372, 2014.

Lee, X., Massman, W. and Law, B. (Eds.): Handbook of Micrometeorology -A Guide for Surface Flux Measurement and Analysis, Kluwer Academic Publishers, Dordrecht, 2004.

Leinweber, A., Gruber, N., Frenzel, H., Friederich, G. E. and Chavez, F. P.: Diurnal carbon cycling in the surface ocean and lower atmosphere of Santa Monica Bay, California, Geophys. Res. Lett., 36, 2009.

Lewis, W. K. and Whitman, W.: Principle of gas absorption, Ind. Eng. Chem., 16, 1215-1220, 1924.

Liss, P. S., and Merlivat, L.: Air-sea gas exchange rates: Introduction and synthesis, in: The role of air-sea exchange in geochemical cycling, Reidel, Boston, 113-129, 1986.

Massman, W. J.: A simple method for estimating frequency response corrections for eddy covariance systems, Agr. Forest Meteorol., 104, 185–198, 2000.

McMillen, R. T.: An eddy correlation technique with extended applicability to non-simple terrain, Bound-Lay. Meteorol., 43, 231–245, 1988.

Mørk, E. T., Sørensen, L. L., Jensen, B. and Sejr, M. K.: Air-Sea CO_2 gas transfer velocity in a shallow estuary, Bound-Lay. Meteorol., 151, 119–138, 2014.

O'Conner, D. J., and Dobbins, W. E.: Mechanism of reaeration in natural streams, Trans. Am. Soc. Civ. Eng., 123, 641-684, 1958.

Pierrot, D., Lewis, E. and Wallace, D. W. S.: MS Excel program developed for CO_2 system calculations. Oak Ridge National Laboratory, Oak Ridge, USA, 2006.

Prytherch, J., Yelland, M. J., Pascal, R. W., Moat, B. I., Skjelvan, I. and Neill, C. C.: Direct measurements of the CO_2 flux over the ocean: Development of a novel method, Geophys. Res. Lett., 37, 2010.

Rutgersson, A., and Smedman, A.: Enhanced air-sea CO_2 transfer due to water-side convection, J. Mar. Sys., 80, 125-134, 2010.

Schindler, D. E., Carpenter, S. R., Cole, J. J., Kitchell, J. F., and Pace, M. L.: Influence of food web structure on carbon exchange between lakes and the atmosphere. Science, 277, 248-251, 1997

Schuepp, P. H., Leclerc, M. Y., MacPherson, J. I. and Desjardins, R. L.: Footprint prediction of scalar fluxes from analytical solutions of the diffusion equation, Bound-Lay. Meteorol., 50, 355–373, 1990.

Tokoro, T., Hosokawa, S., Miyoshi, E., Tada, K., Watanabe, K., Montani, S., Kayanne, H. and Kuwae, T.: Net uptake of atmospheric CO_2 by coastal submerged aquatic vegetation, Glob. Change Biol., 20, 1873–1884, 2014.

564 Tokoro, T., Kayanne, H., Watanabe, A., Nadaoka, K., Tamura, H., Nozaki, K., Kato, K.
565 and Negishi, A.: High gas-transfer velocity in coastal regions with high energy-
566 dissipation rates, J. Geophys. Res- Oceans, 113, 2008.
567 Tsukamoto, O., Takahashi, S., Kono, T., Yamashita, E., Murata, A., and Ishida, H.: Eddy
568 covariance CO_2 flux measurements over open ocean; paper presented at the 13th
569 Symposium on the Interaction of the Sea and Atmosphere, Am. Meteorol. Soc.,
570 8-13, 2004.
571 Vesala, T.: Eddy covariance measurements over lakes, in: Eddy covariance: A practical
572 guide to measurement and data analysis, Springer, Dordrecht, Germany, 365-
573 376, 2012.
574 Vickers, D. and Mahrt, L.: Quality control and flux sampling problems for tower and
575 aircraft data, J. Atmos. Ocean. Tech., 14, 512–526, 1997.
576 Wanninkhof, R.: Relationship between wind speed and gas exchange over the ocean, J.
577 Geophys. Res., 97, 7373–7382, 1992.
578 Watanabe, K. and Kuwae, T.: Radiocarbon isotopic evidence for assimilation of
579 atmospheric CO_2 by the seagrass *Zostera marina*, Biogeosciences, 12, 6251–
580 6258, 2015.
581 Webb, E. K., Pearman, G. I. and Leuning, R.: Correction of flux measurements for
582 density effects due to heat and water vapour transfer, Q. J. Roy. Meteor. Soc.,
583 106, 85–100, 1980.
584 Weiss, R. F.: Carbon dioxide in water and seawater: the solubility of a non-ideal gas,
585 Mar. Chem., 2, 203–215, 1974.
586 Zeebe, R. E., and Wolf-Gladrow, D.: Kinetics. in: CO_2 in Seawater: Equilibrium,
587 Kinetics, Isotope, Elsevier, Amsterdam, 85–140, 2001.

Biogeosciences Discuss., https://doi.org/10.5194/bg-2017-499
Manuscript under review for journal Biogeosciences
Discussion started: 14 December 2017

588 **Table 1.** Summary of the differences in fluxes calculated by the EC and BF methods

	EC	**BF**
Major sources of uncertainty	- Cross sensitivity - Long-term variation (minutes) of CO_2 and water vapor concentrations in air	- Wind-dependent formula - Heterogeneity of measurement site
Measurement location and scales	- CO_2 flux at EC devices - 100 m to km	- CO_2 flux at the air-water surface - < 100 m
Vegetation on the water surface	- effect included	- effect not included
Atmospheric gradient between the measurement height and water surface	- effect included	- effect not included

589
590

Biogeosciences Discuss., https://doi.org/10.5194/bg-2017-499
Manuscript under review for journal Biogeosciences
Discussion started: 14 December 2017

591 **Figure captions**

592 **Figure 1.** Location of the measurement site (Furen Lagoon, Hokkaido, Japan). The
593 lagoon is shallow (1–2 m). Shading indicates seagrass meadows. Eddy covariance (EC)
594 measurements were performed on the platform in 2014.
595
596 **Figure 2**. Post-processing (PP) methods for EC flux calculation. The EC CO_2 flux was
597 calculated by using the conventional PP method (PP1) in EddyPro. The corrections
598 involved in PP1 have been described in previous publications (e.g., Lee et al., 2004).
599 Detrending was performed by using block averaging (BA). Our new PP method (PP2)
600 included three data-filtering steps based on the received signal strength indication of the
601 CO_2 sensor and the standard deviation of the CO_2 and water vapor concentrations
602 divided by the corresponding average standard deviation during the measurement period
603 (nSD). Detrending in PP2 was performed by using high-pass filtering (Massman, 2000).
604
605 **Figure 3.** EC CO_2 fluxes with (a) PP1 (mean: −1.93 μmol m^{-2} s^{-1}, SD: 52.4 μmol m^{-2}
606 s^{-1}, n = 2502) and with (b) PP2 (mean: −0.54 μmol m^{-2} s^{-1}, SD: 2.2 μmol m^{-2} s^{-1}, n =
607 1,833). Several data points in panel (a) are off the scale and not shown for comparison
608 with (b), in which all data are shown. The red line in (b) shows the theoretical maximum
609 negative flux estimated from the BF method (−2.96 μmol m^{-2} s^{-1}).
610
611 **Figure 4.** Instantaneous atmospheric CO_2 concentration (a), water vapor (atmospheric
612 H_2O) concentration (b), and cumulative covariance of atmospheric CO_2 concentration
613 and vertical wind speed calculated with PP1 when the CO_2 fluxes (c) showed the largest

614 positive value (156.5 μmol m^{-2} s^{-1}; blue) and the largest negative value (−217.9 μmol
615 m^{-2} s^{-1}; red). Note that the covariance was not equal to the CO_2 flux because there was
616 no Webb-Pearman-Leuning correction.
617
618 **Figure 5.** Comparison between the effects of the three filtering parameters and the CO_2
619 flux after the RSSI filtering procedure. The red circles indicate the top four outliers for
620 each parameter, which were determined as erroneous (not natural) fluxes. Each
621 threshold (broken red line) was determined so as to remove these data. (a) Normalized
622 standard deviation (nSD = standard deviation over 30-min divided by the average
623 during the entire measurement period; threshold = 0.05; 74 % of data retained). (b)
624 Skewness (threshold = 0.48; 19 % of data retained). (c) Absolute value of kurtosis
625 (threshold = 3.1; 20 % of data retained).
626
627 **Figure 6.** Comparison of CO_2 fluxes calculated by the block averaging (BA) method
628 and EC flux with HP filtering. Most of the data lay on or close to the solid line ($y = x$)
629 and were not much changed by HP filtering. However, in the case of the data in the
630 shaded area, HP filtering decreased the absolute value of fluxes by removing the long-
631 term effect of CO_2 change (see Fig. 7).
632
633 **Figure 7.** Examples of the deviation calculations of atmospheric CO_2 concentration (a)
634 and the cumulative covariance of atmospheric CO_2 concentration and vertical wind
635 speed (b).
636
637 **Figure 8.** Power spectra of CO_2 flux with PP1 and PP2. The spectra were normalized

using the covariances of CO_2 and vertical wind velocity for the entire measurement period after PP1 and PP2. The shaded areas indicate the frequency of the 24-h diurnal cycle (left) and 12.5-h tidal cycle (right). Average CO_2 flux data during the entire measurement period were used to replace missing CO_2 flux data.

Figure 9. Comparison of BF flux, EC flux with PP1, and EC flux with PP2 in May (a), July (b) and September (c).

Figure 10. (a) Relationship between air temperatures and atmospheric CO_2 concentrations. The gray circles indicate the data averaged over 30 min. The open diamonds and error bars indicate the binned averages every 1 °C and 1 SD, respectively. The solid line indicates the slope estimated from the change in air volume assuming that CO_2 behaves as an ideal gas. (b) Relationship and between temperature difference (ΔT) and CO_2 flux. The gray circles indicate the EC flux data calculated every 30 min. The solid diamonds and error bars indicate the binned averages every 1 °C and 1 SD, respectively. Note that for clarity not all data are plotted on both graphs.

Figure 11. Schematic diagram showing the relationships between negative temperature gradient and negative EC CO_2 flux (a) and between positive temperature gradient and positive EC CO_2 flux (b). The atmospheric CO_2 gradient reflects the air temperature gradient and assumes that CO_2 behaves like an ideal gas. The temperature gradient-driven vertical CO_2 flux may explain the discrepancy between the EC and BF fluxes.

Biogeosciences Discuss., https://doi.org/10.5194/bg-2017-499
Manuscript under review for journal Biogeosciences
Discussion started: 14 December 2017

Figure 1

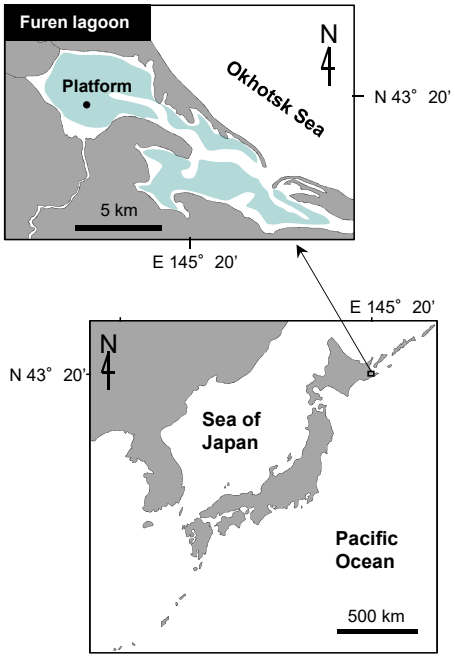

Biogeosciences Discuss., https://doi.org/10.5194/bg-2017-499
Manuscript under review for journal Biogeosciences
Discussion started: 14 December 2017

Figure 2

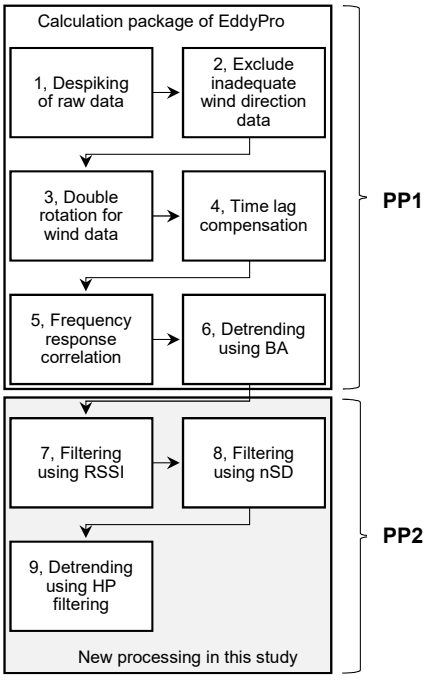

Biogeosciences Discuss., https://doi.org/10.5194/bg-2017-499
Manuscript under review for journal Biogeosciences
Discussion started: 14 December 2017

Figure 3

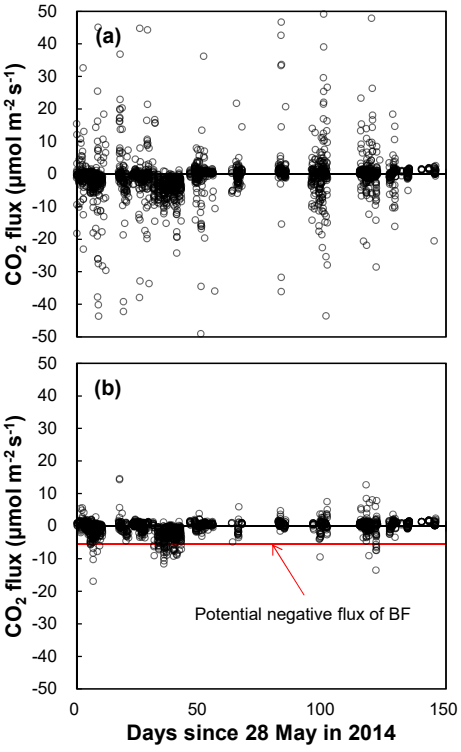

Biogeosciences Discuss., https://doi.org/10.5194/bg-2017-499
Manuscript under review for journal Biogeosciences
Discussion started: 14 December 2017

Biogeosciences Discussions Open Access EGU

Figure 4

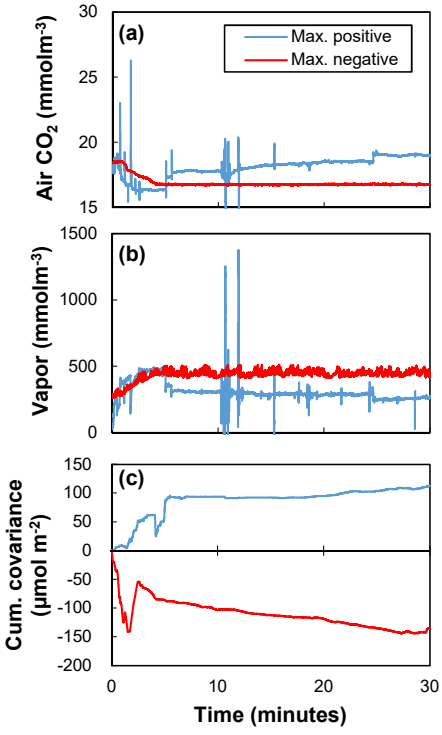

Biogeosciences Discuss., https://doi.org/10.5194/bg-2017-499
Manuscript under review for journal Biogeosciences
Discussion started: 14 December 2017

Figure 5

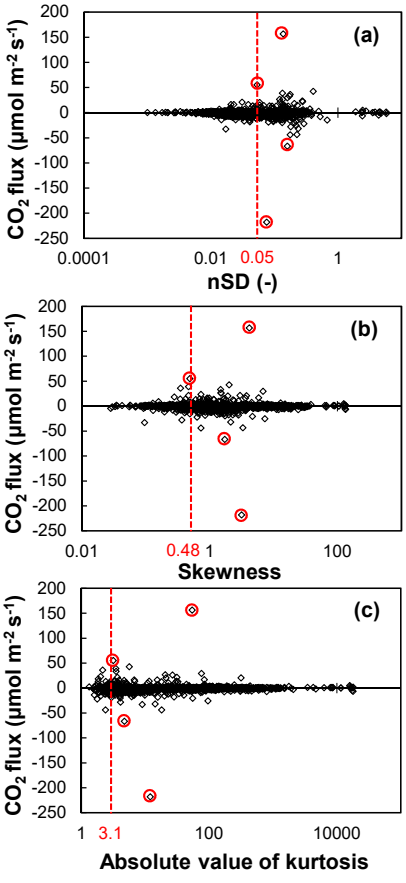

Biogeosciences Discuss., https://doi.org/10.5194/bg-2017-499
Manuscript under review for journal Biogeosciences
Discussion started: 14 December 2017

Figure 6

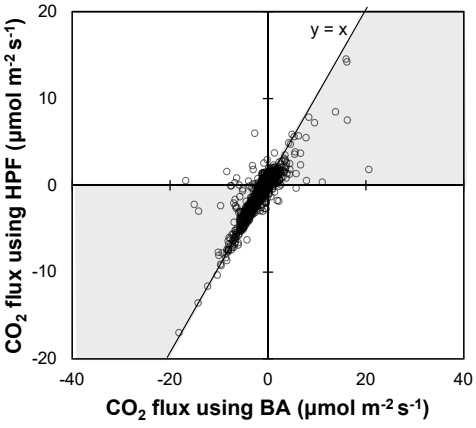

Biogeosciences Discuss., https://doi.org/10.5194/bg-2017-499
Manuscript under review for journal Biogeosciences
Discussion started: 14 December 2017

Biogeosciences Discussions
Open Access
EGU

Figure 7

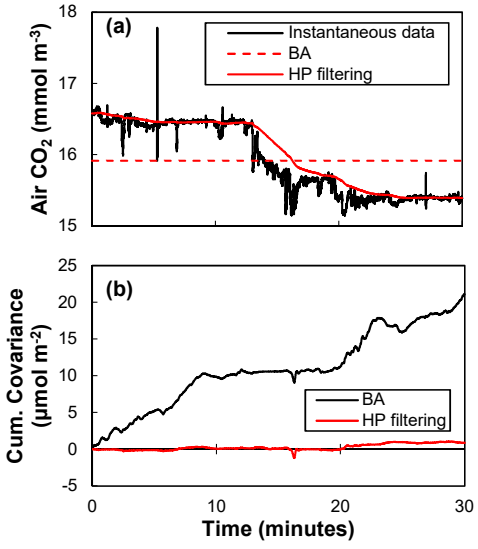

Biogeosciences Discuss., https://doi.org/10.5194/bg-2017-499
Manuscript under review for journal Biogeosciences
Discussion started: 14 December 2017

Biogeosciences Discussions
Open Access
EGU

Figure 8

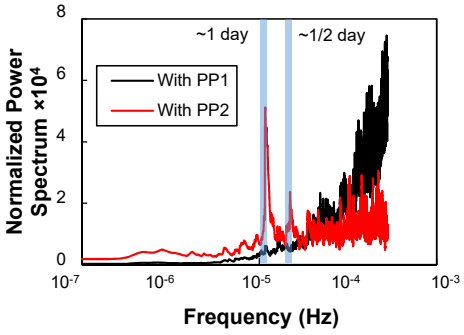

Biogeosciences Discuss., https://doi.org/10.5194/bg-2017-499
Manuscript under review for journal Biogeosciences
Discussion started: 14 December 2017

Figure 9

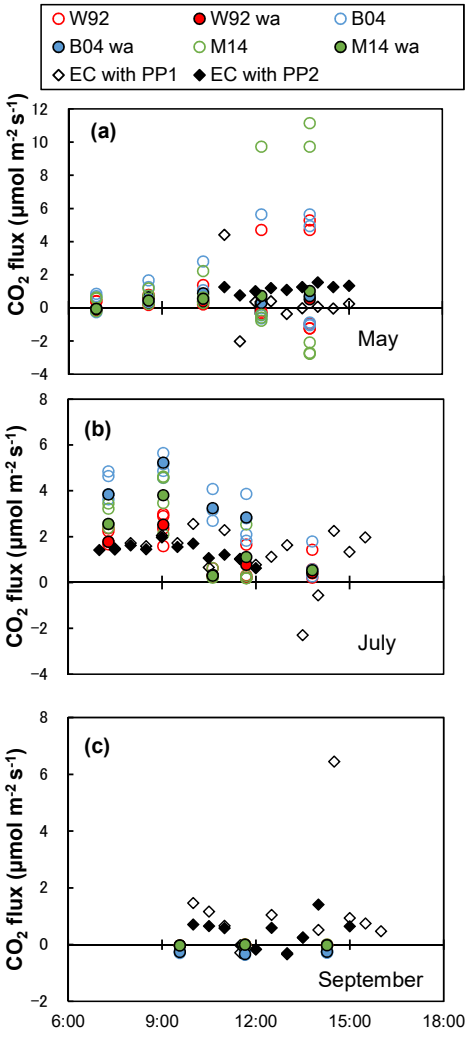

Biogeosciences Discuss., https://doi.org/10.5194/bg-2017-499
Manuscript under review for journal Biogeosciences
Discussion started: 14 December 2017

Biogeosciences Discussions
Open Access
EGU

Figure 10

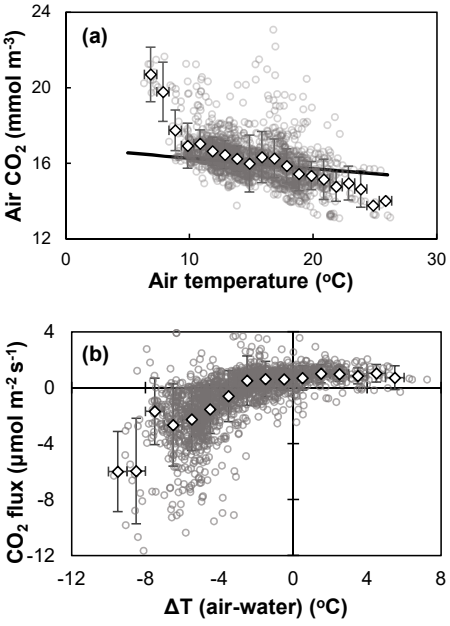

Biogeosciences Discuss., https://doi.org/10.5194/bg-2017-499
Manuscript under review for journal Biogeosciences
Discussion started: 14 December 2017

Figure 11